Structural clusters of histone H3 and H4 residues regulate chronological lifespan in *Saccharomyces cerevisiae*

Mzwanele Ngubo[1§], Jessica Reid[2], Hugh –G Patterton[1,2,*]

[1]Centre for Bioinformatics and Computational Biology, Stellenbosch University, Stellenbosch, South Africa

[2]Department of Biochemistry, Stellenbosch University, Stellenbosch, South Africa

[§]Present address: Ottawa Hospital Research Institute, Regenerative Medicine Program, Ontario, Canada

*Corresponding author. E-mail hpatterton@sun.ac.za, telephone +27 21-8082774

Running title: Histone mutations and chronological lifespan in yeast

Abstract

We have performed a comprehensive analysis of the involvement of histone H3 and H4 residues in the regulation of chronological lifespan in yeast, and identify four structural groups in the nucleosome that influence lifespan. We also identify residues where substitution with an epigenetic mimic extends lifespan, providing evidence that a simple epigenetic switch, without possible additional background modifications, causes longevity. Residues where substitution result in the most pronounced lifespan extension are all on the exposed face of the nucleosome, with the exception of H3E50, which is present on the lateral surface, between two DNA gyres. Other residues that have a more modest effect on lifespan extension are concentrated at the extremities of the H3-H4 dimer, suggesting a role in stabilizing the dimer in its nucleosome frame. Residues that reduce lifespan are buried in the histone handshake motif, suggesting that these mutations destabilize the octamer structure.

All residues exposed on the nucleosome disk face and that cause lifespan extension are known to interact with Sir3. We find that substitution of H4K16 and H4H18 cause Sir3 to redistribute from telomeres and silent mating loci to secondary positions, often enriched for Rap1, Abf1 or Reb1 binding sites, whereas H3E50 does not. The redistribution of Sir3 in the genome can be reproduced by an equilibrium model based on primary and secondary binding sites with different affinities for Sir3. The redistributed Sir3 cause transcriptional repression at most of the new loci, including of genes where null mutants were previously shown to extend chronological lifespan. The transcriptomic profiles of H4K16 and H4H18 mutant strains are very similar, and compatible with a DNA replication stress response. This is distinct from the transcriptomic profile of H3E50, which matches

41 strong induction of oxidative phosphorylation. We propose that the different groups of
42 residues are involved in binding to heterochromatin proteins, in destabilizing the
43 association of the nucleosome DNA, disrupting binding of the H3-H4 dimer in the
44 nucleosome, or disrupting the structural stability of the octamer, each category impacting
45 on chronological lifespan by a different mechanism.

46

Introduction

In an attempt to understand the biochemical context of human diseases of aging such as cancer, diabetes, hypertension and cognitive decline, the regulation of lifespan has been studied as a controlled cellular process[1]. Many interconnected pathways have been implicated in the process of aging[1]. Although there is no clear understanding of the fundamental biochemical mechanism that allows prolonged cellular senescence and extended chronological lifespan, it is known that many of the signaling pathways involved in lifespan extension terminate at induced expression of stress related genes[2].

Calorific restriction is a common trigger in many organisms that feeds into the evolutionary conserved, carbon limitation regulatory pathways such as the TORC1-Sch9 or the Ras1-cAMP-PKA pathways[3,4]. These two pathways converge on Rim15, which translocates to the nucleus when either the TORC1 or Ras1 pathways is inhibited, and facilitate binding of Msn2/Msn4 and Hsf1 to stress responsive and heat shock factor elements, respectively, inducing stress response genes[5]. The mitochondrial retrograde response represents an alternative pathway that signals mitochondrial stress to the nucleus. Here, the Rtg1-Rtg3 complex migrates to the nucleus and binds to R-boxes in conjunction with the SAGA-related SLIK1 acetyltransferase complex, inducing expression of the Rtg responsive genes, including CIT2, that catalyzes citrate synthesis in the glyoxylate cycle. All three pathways have an impact on chronological lifespan (CL) in yeast[6], but the full range of targets of these pathways are not known. Additional pathways that are involved in the regulation of lifespan include the mitochondrial Unfolded Protein Response[7] and induction of autophagy[8].

There is also increasing evidence that epigenetic changes are an integral part of the dynamics of aging[9], both as a result of aging, such as accumulation of H3K27me3 with time[10], and impacting on the regulation of aging[11,12]. These epigenetic changes include histone modifications, histone modifying enzymes and transcription factor localization[12]. The involvement of epigenetics was originally hinted at by the identification of the histone deacetylase, Sir2, in lifespan regulation[13]. Although this identification is now controversial[14], an association between SIRT6 and longevity in rodents was recently reported[15]. Furthermore, both high levels of H3K36 methylation[16] and the substitution of H4K16 was shown to increase replicative lifespan[17]. The yeast silencing complex formed by Sir2, Sir3 and Sir4 was also shown to be important in lifespan regulation[18], suggesting that heterochromatin is involved in this process[11]. Histone H3K4 methylation and H3T11 phosphorylation are the only histone modifications to date shown to affect chronological lifespan (CL) in yeast as opposed to representing a consequence of it[19,20].

It was shown that transgenic mice, where a limited number of double strand breaks (DSBs) were made in the genome by induction of I-PpoI, displayed many features associated with old age at 10 months post treatment, including loss of visual acuity, muscle mass and neurological changes, when compared to an untreated control group[21]. Mouse embryonic fibroblasts derived from the same transgenic mouse line, displayed decreased H3K27ac, and H3K56ac, and increased H3K122ac levels in response to induced DSBs[22]. It was proposed that the repetitive repair of the DSBs causes a redistribution of histone modification marks, triggering the misregulation of a subset of genes that results in accelerated chronological aging[21,22].

Here we focus on the reversed question, asking what the impact of histone modifications and epigenetic marks are on aging, as opposed to what epigenetic marks change as a result of aging. We identify categories of histone H3 and H4 residue substitution that impact on extension or reduction of CL, and demonstrate that substitutions with a profound impact on lifespan extension may act through very different signalling pathways and transcriptomic programmes.

Results

Identifying histone H3 and H4 residues involved in the regulation of lifespan

We studied approximately 400 barcoded, non-lethal, synthetic histone H3 and H4 mutants in *Saccharomyces cerevisiae*[23], to gain an insight into the role of histone modifications in the regulation of CL. Each residue was systematically substituted with an alanine or a residue that mimicked the unmodified and modified state of an epigenetic switchable residue[23]. A culture that initially contained an equal level of each histone mutant strain was maintained in stationary phase for 55 d, quiescent cells isolated, and the level of each strain determined by independent quantitation of two DNA barcodes at progressive times. Quiescent cells were used to quantitate the level of healthy cells that were aging, as opposed to non-quiescent cells that were dying and had initiated apoptosis[24]. This "bar-seq" approach was previously shown to accurately quantitate individual strains in a mixture of barcoded yeast strains in culture[25]. We found that the level of some strains decreased at a lower rate, and others at a faster rate, compared to the population median or the parental WT (Figure 1**a**). The results of the quantitation by barcode sequencing are given in Supplementary Table 1. Although extended culturing of yeast in stationary phase

increases acetic acid levels in the medium, this extended culturing is appropriate for studying CL, since it was shown that yeast faithfully reproduced responses and induction of pathways associated with chronological aging observed in other model organisms that were not exposed to elevated levels of acetic acid[26].

Residues with the largest impact on chronological lifespan extension are exposed on the nucleosome disk face

The 10 individual residues that caused the most pronounced lifespan extension (red residues in Fig. 1**a,c**) are all located either in the H4 tail or exposed on the solvent accessible face of the nucleosome, within the sectors previously identified as the Swi/Snf independent (Sin) or the Loss or rDNA silencing (Lrs) sectors at SHL±0.5 and ±2.5[27].

H4K16 Q and R substitutions were previously shown to prolong replicative aging[17]. We have identified H4K16 as a residue also implicated in chronological lifespan extension (CLE) (Supplementary Table 1). Interestingly, any mutation of H4K16 (to Q, R, or A) cause an increase in CL (Supplementary Table 1), suggesting that a lysine residue is specifically required at position 16 for normal CL. This suggestion is supported by the observation that both the H4Δ9-16 and H4Δ12-16 tail deletions extend lifespan (Figure 1**i** and Supplementary Table 1). Interestingly, the H4 tail deletions Δ1-12 extended CL, whereas the short N-terminal deletion Δ1-4 reduced lifespan, demonstrating that the combined loss of H4 residues 5-12 were sufficient to abrogate the negative effect of loss of residues 1-4 (Figure 1**i** and Supplementary Table 1). This is supported by the extended lifespan observed for the Δ5-12 H4 deletion (Figure 1**i** and Supplementary Table 1).

The solvent exposure of the top 10 individual residues where mutation prolong lifespan suggests that these residues are involved in binding to a protein on the surface of the nucleosome disk. It is known that H4K16, H4H18, H4L22, H4N25, and H3T80, identified in the strains with extended lifespan, all interact with the Sir3 BAH domain[28,29]. Sir3 is involved in establishing transcriptionally repressive heterochromatin at the telomeres and silent mating type loci. The only residue in this solvent exposed group that is not known to interact with the BAH domain is H3E50. H3E50 is exposed on the lateral surface of the nucleosome core between two DNA gyres (Figure 1**c,d**), suggesting that H3E50 may influence the regulation of yeast lifespan through a different, Sir3-independent pathway. H3E50 makes an H-bond to H4R39 in α1 of H4, which could contribute to placing the N-terminal tail of H3 in the correct radial position in the nucleosome (Supplementary Fig. 1**a**).

The top 10% of residues that cause moderate chronological lifespan extension are concentrated at the H3-H4 dimer extremities

Strikingly, the top tenth percentile of residues associated with prolonged CL, excluding those on the solvent exposed face of the nucleosome and H3E50, are concentrated at the extremities of the histone fold domain (violet residues in Fig. 1**a**). Residues in this category appear to be concentrated at the H3 α3 C-terminus, the C-terminal region of α2 and L2 of H3, the N- and C-terminal regions of α1 and L1 of H3, the N-terminal region of H4 α2, bracketing the H4 L2 at the C-terminus of α2 and N-terminus of α3, and in the region where H4 α1 passes over H3 αN (Fig. 1**b,c**). The interactions of these residues specifically exclude the extensive interactions between dimer partners,

and seem enriched for contacts that stabilize the conformation of the histone fold domain and the H3-H4 dimer in its frame within the nucleosome structure (see Supplementary Note). It is not immediately clear what the impact of mutations at these positions are on dynamic nucleosome structure.

Residues implicated in a reduced CL are buried, and may destabilise the octamer

The positions of the mutated residues in the ten strains with most reduced lifespans (Fig. 1**e**) in the quiescent pool are shown in Fig. 1**f,g**. Most H3 tail deletions, including the short N-terminal deletion Δ1-4, resulted in reduced lifespan, showing that an intact H3 tail is required for normal lifespan (Figure 1**i** and Supplementary Table 1). In contrast, short internal H3 tail deletions Δ17-24, Δ24-28 and Δ29-32 extends lifespan (Figure 1**i** and Supplementary Table 1). The first two of these short deletions bracket the residues K23 and K27, both in the top 10% of residues that extend lifespan when mutated (Figure 1**i** and Supplementary Table 1). Notably, substitution of four histone H3 tail lysine residues with arginine (H3K4, 9, 14, 18R) reduce lifespan. Either this suggests that mimicking a constitutively deacetylated state for these lysine residues decreased lifespan, or that a modifiable lysine is required for normal lifespan. The latter seems likely, since the H3K18Q mutant, mimicking a constitutive acetylated state, also exhibits a shortened lifespan (Supplementary Table 1). In addition, deletion of Set1, which abrogates methylation of H3K4, decreased CL, and, conversely, deletion of the H3K4me3 demethylase, Jhd2, increased CL[19], arguing that a modifiable H3K4 residue is necessary for a normal CL.

The location of the residues where mutations decreased lifespan is summarized in Fig. 1**f,g**. It is striking that, unlike the solvent exposed residues (Fig. 1**b,c**) or residues implicated in stabilizing each H3-H4 dimer in a structural frame (Fig. 1**b,c**), all residues implicated in a shortened lifespan, except for the H3 N-terminal tail mutations, are buried within the octamer structure, and occur between interacting sections of the histone fold domains (Figure 1**f,g**). We speculate that the mutations that cause a shortened lifespan contribute to the structural destabilization of the histone octamer and disruption of nucleosomes and chromatin structures (Supplementary Note). It was previously shown that reducing histone H3 and H4 levels, and presumably nucleosome density, resulted in a reduced CL[30].

We verified the results of the barcode approach by confirming the survival of select strains implicated in lifespan regulation in biological replicates (Figure 2). The reproducibility of the observed lifespans also shows that the result of the bar-seq quantitation does not simply reflect the population variance of a random process.

The H4K16 and H4H18 mutants cause re-distribution of Sir3 in the genome

The solvent exposed residues H4K16, H4H18, H4L22, H4N25 and H3T80 all interact with the BAH domain of Sir3 in the crystal[28], and substitution of these residues cause CLE. These substitutions are expected to disrupt the binding of Sir3 on the side of the nucleosome[28,29]. To investigate the effect of mutation of these residues on the genomic distribution of Sir3, we performed a ChIP-seq analysis of H4K16Q, H4H18A and H3E50A mutants. These mutations were selected to include one residue previously implicated in lifespan extension, H4K16, albeit replicative lifespan[17], a residue newly

199 identified to cause CLE, H4H18, and a residue similarly shown to cause CLE, but unlikely
200 to be involved in direct Sir3 binding, H3E50.

201 After incubating cultures for 6 d, the Sir3 occupancy at HMLα and HMR**a** were
202 found to be reduced by at least two-fold in the H4K16Q and H4H18A mutants, and to
203 approximately 80% of the WT level at HMLα in the H3E50A mutant strain (Figure 3**a,b**).
204 In a WT cell Sir3 was enriched at the telomere X element and the borders of the Y'
205 element, as previously reported[31]. Sir3 binding was reduced at the X elements in the
206 H4K16Q, H4H18A and H3E50A strains, but remained at levels comparable to the WT at
207 the Y' element (Figure 3**c**). When looking at Sir3 distribution throughout the whole
208 genome, it is seen that the levels of Sir3 at the terminal 20 kb of chromosomes,
209 normalised to the genome, are significantly lower (*t*-test, $p < 0.05$) in the H4K16Q and
210 H4H18A mutants compared to the WT (Figure 4). There is no significant difference in
211 Sir3 telomeric levels between the WT and the H3E50A mutant, but there is a significant
212 difference between the levels between the H4K16Q or H4H18A mutant and the H3E50A
213 mutant (*t*-test, $p < 0.05$). A similar pattern of differences is seen between the Sir3 levels
214 at the chromosome cores, excluding the terminal 20 kb (Figure 4). This demonstrates
215 that Sir3 is redistributed from the telomeres to the chromosome cores in the H4K16Q and
216 H4H18A mutants. This may reflect a migration from a compromised nucleosome binding
217 site to secondary binding sites in the genome with binding affinities that are now
218 competitive with the mutant nucleosome. No significant change in the telomeric
219 distribution of Rap1, which recruits Sir3 to the telomeres to form silent heterochromatin[31],
220 is seen when comparing the H4H18A mutant to the WT strain, underlining the fact that
221 Rap1 binds to DNA[32] whereas Sir3 associates with nucleosomes (Fig 5). It was

previously shown that Rap1 redistributed from the telomeres to internal sites in a *Δtlc1* strain with shortened telomeres, which was proposed to represent an aged senescent cellular state[33]. However, this relocation was likely due to decreased Rap1 binding sequence and not simulated age, since we saw no evidence of such a reorganization with chronological aging over a 14 d period (Supplementary Fig. 2).

Re-distributed Sir3 is associated with transcriptional repression at the new loci.

Sir3 peaks were identified in the ChIP-seq data of the mutant strains. To assess whether the redistributed Sir3 repressed transcription in the newly occupied regions, we analysed the differential expression of genes in the mutant strains relative to the WT when the transcribed gene, including a 500 bp upstream region, overlapped with the identified new Sir3 peak. In the H4K16Q mutant, 33 genes overlapped with Sir3 peaks, of which 22 genes were repressed compared to the WT. Given that 48% of the quantitated genes in the complete RNA-seq data set were down-regulated, a binomial probability distribution function of $\binom{33}{22}\times 0.48^{22}\times 0.52^{11} = 0.01$ is obtained. Thus, there is only a 1% chance that random selection of 33 genes from this RNA-seq data set will include 22 down-regulated genes, strongly suggesting that the redistributed Sir3 indeed represses gene expression at most of the newly occupied loci.

There is no unique transcription factor binding site associated with all re-distributed Sir3 peaks. Importantly, Sir3 peaks were not always associated with an ARS consensus sequence, found in the E elements of the HM cassettes. We calculated the significance of the presence of factor binding sites in Sir3 peaks given the number of such factor sites in the genome, and assuming a Poisson probability distribution (Supplementary Table 2).

It seems that Sir3 distributes to a number of sites, recruited by a combination of factors including Abf1, Rap1 and other factors (Supplementary Table 2). It therefore appears likely that Sir3 redistributes to a number of diverse secondary binding sites in the genome in the H4K16 and H4H18 mutant strains.

Considering the genes associated with Sir3 peaks in the mutant strains, we found that the YIL055C gene is common to all three extended CL mutant strains (Supplementary Fig. 3 and Supplementary Table 3). YIL055C encodes a protein of unknown function that is associated with the mitochondrion and interacts genetically with the histone deacetylases Hda1 and Hos1, subunit 8 of ubiquinol cytochrome-c reductase (Complex III), the β-subunit of the Sec61-Sss1-Sbh1 ER translocation complex, actin and Cdc13, the telomere repeat binding protein involved in the regulation of telomere replication. A *Δyil055c* strain is, however, not associated with CLE[34,35].

The redistributed Sir3 peaks of the H4K16Q and H4H18A mutant strains commonly cover MAM3, encoding a protein associated with the ER membrane that is required for mitochondrial morphology, and SND1, encoding a protein involved in alternative ER targeting. Again, neither *Δmam3* nor *Δsnd1* strains are associated with CLE[34,35] (Fig. 6).

It was previously shown that the propagation and termination of repressive heterochromatin domains occur with a degree of randomness that is the basis for position effect variegation [36]. It is thus expected that the exact positions of the new loci associated with Sir3 will differ between cells and between strain, which could allow different genes that have an impact on the regulation of lifespan to be repressed in the otherwise identical H4K16 and H4H18 mutant strains. The GDH1 glutamate dehydrogenase gene is

repressed in the H4K16 mutant strain, and is associated with a CLE phenotype in a null strain[34]. In the H4H18 mutant strain the AGP1, HTZ1 and SHR5 genes, encoding a glutamine transporter, the histone H2A.Z, and a palmitoyltransferase that suppresses Ras1 function, are associated with new Sir3 loci, and were all shown to be associated with CLE phenotypes in null mutants[34,35]. The redistributed Sir3 is thus associated with genes that were previously shown to confer extended CLs in null mutants, and could provide a simple, causative link between Sir3 redistribution and lifespan expansion.

The H4K16Q and H4H18A mutants have similar transcription profiles that differ from that of H3E50A

Although it is possible that the repression of one or a few genes by redistributed Sir3 may impact on the expression of a central and important component in a pathway involved in the regulation of CL, and single genes identified above may contribute to lifespan extension, we note that the transcriptomic profile of the CLE strains differ from that of the WT strain at hundreds of genes. It is thus likely that the histone mutations also have gene regulatory effects other than Sir3 binding, or that the redistribution of Sir3 in the genome have indirect effects that impact on many additional genes, some of which are involved in CLE. We therefore analysed the RNA-seq data of three CLE strains to attempt to identify functional GO categories or pathways that presented an additional possible mechanistic basis for the observed extended CL.

Gene expression is significantly down-regulated in stationary phase[37]. Although the expression or repression of specific genes in stationary phase may support CLE, we were interested in the transcription programme that preceded stationary phase, and that may

prepare a biochemical state that allowed subsequent extended CL in stationary phase. For this reason, we performed RNA-seq analyses on cultures in late log phase.

The H4K16 and H4H18, H4K16 and H3E50 and H4H18 and H3E50 RNA-seq datasets have Spearman rank correlation coefficients of 0.7, -0.04 and -0.2 respectively, showing that H4K16 and H4H18 are most closely related, and that the H3E50 profile has little correlation to either of the H4 mutant strain sets.

An analysis of the GO terms for biological processes enriched for the genes that are induced in the H4K16Q strain (adjusted $p<0.05$) compared to the WT show a significant enrichment for biosynthetic processes, cytoplasmic translation, ribosome biogenesis and RNA processing (Supplementary Table 4). The largest number of induced genes further map to pathways involved in the biosynthesis of secondary metabolites and amino acids, ribosome biogenesis, RNA transport and purine metabolism (Supplementary Table 5). Genes that are down regulated in the H4K16Q strain (adjusted $p<0.05$) are associated with DNA integration, recombination and biosynthetic processes, as well as mitochondrial respiratory chain complex assembly (Supplementary Table 6). Down regulated pathways include metabolic, cell cycle, MAPK signalling, autophagy and carbon metabolism pathways (Supplementary Table 7). It thus appears that in late log the cell is actively synthesizing proteins, but shutting down oxidative phosphorylation and DNA synthesis. A very similar pattern of regulated genes and enriched GO functional categories and pathways was observed for the H4H18A strain (Supplementary Tables 4-7).

In contrast, the H3E50A mutant shows increased expression of genes associated with oxidation-reduction processes, generation of precursor metabolites, energy derivation by

oxidation of organic compounds, tricarboxylic acid cycle and the electron transport chain (Supplemental Table 4). Enriched pathways include carbon metabolism, tricarboxylic acid metabolism, respiratory electron transport chain, oxidative phosphorylation and autophagy (Supplemental Table 5). Down regulated genes include the GO functional categories of ribosome biogenesis, cytoplasmic translation, RNA processing (Supplementary Table 6), ribosome biogenesis, cell cycle, and purine metabolism pathways (Supplementary Table 7).

The transcriptomic profile of the H3E50A mutant strain is essentially the inverse of the H4K16Q and H4H18A strains. Protein synthesis is down regulated, and the tricarboxylic acid cycle and the oxidative phosphorylation is activated. It thus appears that the H3E50A strain is actively synthesizing ATP by oxidative phosphorylation in late log phase. MSN4, CIT2, SOD1 and SOD2 are all significantly induced in the H3E50A strain, suggesting that the mitochondrial retrograde response is active, and that the yeast cell is responding to oxidative stress and inducing Msn4 responsive stress genes. It is surprizing that the mutation of a single residue that stabilises the position of the N-terminal tail of histone H3 in the nucleosome induces a mitochondrial retrograde response or related transcriptomic effect. The H4K16Q and H4H18A strains display elevated MSN2/4 expression levels, but decreased CIT2, SOD1 and SOD2 levels, suggesting the absence of the retrograde response, and the presence of a general stress response in these mutant strains.

Discussion

We have identified four groups of H3 and H4 residues situated in different regions of the nucleosome where substitution have an impact on CL. The location of each group

provides a hint of the possible mechanistic route by which it influences CL. The first group consists of residues exposed to the solvent on the face disk of the nucleosome and present in the N-terminal tails. The residues on the face disk are involved in binding to the Sir3 heterochromatin protein and cause a pronounced extension of CL. The operative substitution of these residues do not necessarily represent valid epigenetic switches. H4K16, for example, confers CLE when substituted with either R, Q or A. It seems that an unmodified K residue stabilises binding to Sir3 by forming a hydrogen bond between the ε–amino group and the S67 hydroxyl in the BAH domain of Sir3[28], an association that is necessary for a normal CL. Any alteration disrupts this H-bond, irrespective of whether it is an epigenetic mimic or not, and extends CL. Another example is H4H18, a residue that was also shown to interact with Sir3 by formation of an H-bond between the imidazole imino group and E95 in the BAH domain[28]. H4H18 extents CL when mutated to an A, which does not represent a valid epigenetic state switch.

H3T11, on the other hand, present in the N-terminal tail of H3, extends CL when substituted with D, a mutation that mimics constitutive phosphorylation. The WT residue and the H3T11A mutant exhibit a CL similar to that of the population average. This category of residue is of acute interest, since it represents an epigenetic mark where transition between different epigenetic states modulate CL.

The second group of residues in the nucleosome is defined by the single member, H3E50. This residue, like the members of the first group, causes prolonged CL when mutated, but is not involved in binding to Sir3. The WT residue makes an H-bond to an amino group in H4R39, and contributes to setting the exit position of the H3 N-terminal tail in the

354 nucleosome. When substituted in the H3E50A mutant, CL is extended. It was previously
355 shown that the H3E50A mutant has a double strand break checkpoint defect[38],
356 suggesting an alternative mechanistic pathway by which a histone residue can effect
357 CLE.

358 The third group of residues are clustered at the extremities of the histone folds of H3 and
359 H4, at L1 and L2, and are likely to be involved in stabilizing the conformations of the α1
360 and α3 helices relative to α2, as well as binding to the DNA duplex. These residues may
361 be involved in stabilizing the H3-H4 dimer in its structural frame in the nucleosome. It is
362 possible that substitutions at the L1 and L2 positions influence H3-H4 dimer binding in
363 the nucleosome, and are likely to have a pleiotropic effect and an impact on diverse
364 functionalities of chromatin. This category of substitution is likely to confer CLE through
365 several pathways, since it may involve disparate functions of the genome. Residues in
366 group three typically extend CL to a lesser degree than residues in groups one and two.

367 The fourth category is composed of residues buried within the octamer, and are likely
368 involved in stabilizing the histone octamer itself. Residues in the fourth category are
369 exclusively associated with a shortened CL when substituted. We postulate that these
370 mutations disrupt the structural stability of the nucleosome, a fundamental structural unit
371 of chromatin, and may accelerate apoptosis. It was previously shown that loss of histone
372 H3 and H4 reduced CL[39].

373 The Workman group showed that H3T11 was phosphorylated by both Sch9 and Cka1,
374 and reported that *Δsch9* and *Δcka1* as well as H3T11A prolonged CL[20]. Although this
375 seems opposite to our result where the phosphorylated mimic H3T11D showed CLE, we

note that the *Δsch9* mutant strain will facilitate activated expression of Msn2/4 stress response genes associated with CLE[40], and it is not clear if the CLE observed was due to absence of H3T11 phosphorylation or induction of stress response genes. A phosphorylated mimic H3T11D was not tested[20].

A SPELL analysis[41] showed that both the H4K16 and H4H18 mutant gene expression profiles were most closely related to that of yeast strains under conditions of carbon and nitrogen stress or DNA replication stress. Importantly, neither the H4K16 nor H4H18 mutant strain exhibited a gene expression profile similar to a *sir3Δ* strain. The H3E50 transcriptomic profile matches most closely sets related to stationary phase entry, carbon utilization, diauxic shift, fermentation and respiration.

A search of the HistoneHits database[42] of the classic phenotypes associated with histone mutants showed that H3E50A was associated with a modest decrease in the DNA damage phenotype. H4K16A and H4K16Q showed decrease in telomeric silencing and mating efficiency, and H4K16A, H4K16Q and H4K16R showed HM cassette derepression. H4H18A and H4H18Q displayed defects in HM and telomeric silencing. The majority of H4 tail deletions between 1 and 28 exhibited HM cassette silencing defects. We note that although chronological aging is associated with HM derepression, derepression of HM per se does not cause chronological aging[43].

We propose that the redistribution of Sir3 to alternative sites in the genome is caused by a change in the affinity of the binding site on the face of the nucleosome disk for the Sir3 BAH domain, due to the substitution of an interacting histone residue. In *S. cerevisiae*, heterochromatin is typically initiated by the recruitment of a heterochromatin protein such

as Sir1 to a DNA-bound initiation factor such as Orc1[44]. The heterochromatin domain is propagated by the binding of a modifying enzyme such as the Sir2 deacetylase to the heterochromatin initiation core, deacetylation of H4K16ac of the adjacent nucleosome, binding of the heterochromatin protein complex Sir3/Sir4 to the modified nucleosome, and re-recruitment of Sir2 by the newly deposited Sir3/Sir4. The continuous, repetitive modification of each adjacent nucleosome and subsequent binding of Sir3/Sir4 leads to the progressive extension of the heterochromatin domain along the DNA[45,46].

Both the initiation factor as well as the nucleosome contribute to define a binding affinity, and this initial affinity will influence successive binding affinities in the propagated heterochromatin domain due to contact between the neighbouring Sir3/Sir4 sub-units[46]. This propagation continues with a defined probability with every consecutive, interacting Sir3/Sir4 sub-unit, or until firm termination by an insulator, TFIIIC bound to a pol III gene A-box[47] or a euchromatic domain defined by an epigenetic modification such as H3K79me3[48] or the enrichment of histone variant Htz1[49].

We did not detect any transcription factor binding site that was invariably associated with the redistributed Sir3 domains in the mutant strains. A range of sites were linked to the new loci, suggesting that Sir3 is recruited to different regions of the genome by a number of different or even a mixture of initiator factors such as Abf1 and Rap1, known to bind to Sir3[50]. These secondary binding sites will also have an affinity defined by a combination of the recruiting factor and the binding site on the nucleosome face.

The binding of Sir3 to a high affinity, primary site, such as an HM locus, can be described by the equilibrium equation

$$[P] + [B_1] \rightleftharpoons [PB_1] \qquad \text{(equation 1)}$$

where $[P]$ and $[B_1]$ represents the concentrations of Sir3 and the nucleosome binding site, respectively, and $[PB_1]$ is Sir3 bound to the binding site. The association constant K_{a1} is defined by

$$K_{a1} = \frac{[PB_1]}{[P][B_1]} \qquad \text{(equation 2)}$$

Similarly, the binding to a low affinity, secondary binding site can be represented by

$$[P] + [B_2] \rightleftharpoons [PB_2] \qquad \text{(equation 3)}$$

where $[B_2]$ represent the concentration of the secondary binding site and $[PB_2]$ is bound Sir3.

The fractional binding f_{PB_1} of Sir3 associating with the primary site B_1, assuming that $[P]$ is limiting, thus $[P]$ << $[B_1]$, is given by

$$f_{PB_1} = \frac{[PB_1]}{[P]+[PB_1]+[PB_2]} \qquad \text{(equation 4)}$$

$$= \frac{K_{a1}\cdot[P]\cdot[B_1]}{[P]+K_{a1}\cdot[P]\cdot[B_1]+K_{a2}\cdot[P]\cdot[B_2]} \qquad \text{(equation 5)}$$

Fractional binding of Sir3 to the secondary site B_2 is similarly given by

$$f_{PB_2} = \frac{[PB_2]}{[P]+[PB_1]+[PB_2]} \qquad \text{(equation 6)}$$

$$= \frac{K_{a2}\cdot[P]\cdot[B_2]}{[P]+K_{a1}\cdot[P]\cdot[B_1]+K_{a2}\cdot[P]\cdot[B_2]} \qquad \text{(equation 7)}$$

Assuming that $[B_1] \approx [B_2] = [B]$, which appears likely, judged by the comparable number of Sir3 peaks observed in the WT and the mutant strains, gives

$$f_{PB_1} = \frac{K_{a1}\cdot[B]}{1+[B]\cdot(K_{a1}+K_{a2})} \approx \frac{K_{a1}}{K_{a1}+K_{a2}} \text{ if } B >> 1 \qquad \text{(equation 8)}$$

$$f_{PB_2} = \frac{K_{a2}\cdot[B]}{1+[B]\cdot(K_{a1}+K_{a2})} \approx \frac{K_{a2}}{K_{a1}+K_{a2}} \text{ if } B >> 1 \qquad \text{(equation 9)}$$

Setting K_{a1} and K_{a2} of the high and low affinity binding sites equal to 50 μM^{-1} and 10 μM^{-1}, implies a $f_{PB_1} = {}^{5}/_{6}$ and $f_{PB_2} = {}^{1}/_{6}$. The high affinity binding sites are thus bound at a 5-fold higher level than the low affinity binding sites. If the K_{a1} in the mutant strain is decreased by 5-fold from 50 to 10 μM^{-1} due to the disruption of the Sir3 binding surface on the nucleosome face, and K_{a2}, representing a different initiator factor in combination with a nucleosome face, is reduced 2-fold from 10 to 5 μM^{-1}, $f_{PB_1} = {}^{4}/_{6}$ and $f_{PB_1} = {}^{2}/_{6}$. Thus, a 20% reduction in binding to the primary site and a 100% increase in binding to a secondary site will be evident.

We propose that we observe a related binding scenario in the mutant strains. A lesser reduction in the binding affinity to secondary sites causes a displacement of Sir3 from the high affinity binding sites in the WT, to weaker secondary binding sites. These have binding affinities in the same order of magnitude as the compromised primary binding sites in some mutant strains. This allows the redistribution of Sir3 to secondary sites that are randomly distributed throughout the genome, fortuitously repressing genes near the

454 new loci, including genes where null mutants were implicated in CLE. We therefore
455 propose that the redistribution of heterochromatin domains are not mechanistically
456 directly responsible for an extended lifespan, but that the incidental repression of genes
457 that regulate lifespan cause the observed CLE.

458 # Methods

459 ## Yeast strains and media

460 The histone mutant library, constructed by the Boeke group [23], and based on the parental
461 strain JDY86 (*MATa, his3Δ200, leu2Δ0, K2Δ0, trp1Δ63, ura3Δ0*, *met15Δ0,*
462 *can1::MFA1pr-HIS3, hht1-hhf1::NatMX4, hht2-hhf2::[HHTS-HHFS]-URA3*, where
463 *[HHTS-HHFS]* designates the mutated histone which is either H3 or H4) was purchased
464 from Thermo Fischer Scientific. YPD yeast growth medium was prepared with 1% (w/v)
465 yeast extract, 2% (w/v) peptone and 2% (w/v) glucose. Agar-YPD contained 2% (w/v)
466 bacto-agar. All media were sterilized by autoclaving before use, and all chemicals were
467 molecular biology grade.

468 ## Culturing of the pooled library

469 The histone H3 and H4 mutant library was replica plated onto omnitray YPD-agar plates,
470 and selected with 200 ng/ml nourseothricin (Sigma) antibiotic. Colonies were grown for
471 2-3 days at 30°C. Slow-growing colonies were separately streaked out from the original
472 stock, and grown for 2-3 days at 30°C. The contents of all the plates, including the slow-
473 growers (equivalent volume of a normal colony) were scraped off, and pooled in a 50 ml
474 conical centrifuge tube containing YPD liquid media with 200 ng/ml nourseothricin. The

pooled culture was diluted to a final concentration of OD_{600} = 50, 15% (v/v) glycerol was added, and stored as aliquots at -80°C.

The pooled culture was inoculated into 100ml YPD liquid media to a final concentration of OD_{600} ~ 0.003. Cells were grown with rotary shaking (180 rpm) at 30°C for approximately 10 generations (~15 h). The pooled culture was then further diluted to OD_{600} of 0.06 in 250 ml YPD liquid media, and incubated for up to 55 d with continual shaking (180 rpm) at 30°C. Aliquots (10 ml) were recovered at the times indicated.

Bar-code sequencing

Culture aliquots were washed twice with 5 ml water, the cells resuspended in 1 ml of 50 mM Tris-HCl (pH 7.5), and carefully overlaid onto a performed Percoll gradient [24], and centrifuged at 400 g, 60 min, 20°C in a GH-3.8 swinging bucket rotor (Beckman). Quiescent cells were collected with a Pasteur pipette and washed once with 30 ml of 50 mM Tris-HCl pH 7.5 at 650 g, 5 min, 20°C in a GH-3.8 swinging bucket rotor. Genomic DNA was isolated from 1 ml quiescent fractions (YeaStar kit, Zymo Research, Protocol I), and the DNA eluted with 60 μl of TE buffer (10 mM Tris-HCl pH 8.0, 0.1 mM EDTA), and stored at -80°C. The “up” and “down” bar-code sequences were separately amplified in two reaction volumes containing 50 ng of genomic DNA, 0.3 μl of 5 U/μl FastStart Taq DNA polymerase (Roche), 0.4 μl of 100 μM “up” or “down” barcode primer pair, 0.5 μl of 10 mM dNTP, 12 μl of 25 mM $MgCl_2$, 3 μl of 10x PCR buffer without $MgCl_2$, and water to in a final volume of 30 μl. The primer sequences were ATGTCCACGAGGTCTCT, CCTCGACCTGCAGCGTA, CGGTGTCGGTCTCGTAG, and CCCAGCTCGAATTCATC for “up”, forward and reverse, and “down”, forward and reverse, respectively. The amplified DNA was purified[51], quantitated, single-end adapters with index primers

(Illumina) ligated to each sample, and single-end sequenced on a HiSeq 2500 (ARC Biotechnology Platform, University of Pretoria).

The number of times that each barcode sequence was present in the FASTQ file was assessed for "up" and "down" barcodes with *get_seqs_from_fastq* for each time point, quantitated with *match_barcodes_to_strain*, and the average of the "up" and "down" value, adjusted for the amplified DNA signal, expressed as the $\log_2$ ratio relative to the level in the mixed starting population. The code is available at github.com/hpatterton. The data was deposited in the NCBI GEO archive (accession number GSE140160).

Verification of chronological lifespan

To verify the results of the barcode analysis, 250 ml of YPD liquid media was inoculated to an OD_{600} of 0.06 with starter cultures of selected mutant strains, and incubated for up to 50 d at 30°C with shaking (180 rpm). Aliquotes (100 µl) of cells were recovered at sequential times, serially diluted onto YPD-agar plates, and the number of colony forming units (CFU/ml) determined after incubating for 2 d at 30°C. Biological replicates were quantitated.

RNA-seq

Total RNA was isolated from 10 ml cultures of yeast strains and purified with an RNeasy kit (Qiagen). The RNA was prepared for sequencing using the TruSeq Stranded Total RNA Sample Prep adaptor kit (Illumina). The samples were sequenced on a HiSeq 2500 instrument (Illumina) using the 100 nt paired-ends sequencing protocol. Biological replicates of each sample were independently prepared, sequenced and analysed.

519 The quality of the sequence reads was assessed with FastQC, and reads trimmed and
520 filtered for a minimum Q score and length with Trim Galore. Reads were mapped to
521 version 64 of the reference yeast genome (www.yeastgenome.org) with RNA STAR. The
522 number of mapped reads per gene was counted with featureCounts, and differential
523 expression quantitated with edgeR. The RNA-seq data was deposited in the NCBI GEO
524 archive (accession number GSE141975).

525 **ChIP-seq**

526 Cultures (50 ml) were cross-linked in 1% (v/v) formaldehyde for 20 m, 25°C, and the
527 reaction quenched with glycine (125 mM), 5 m, 25°C. The cells were washed once in 50
528 ml PBS (pH 7.4), and resuspended in lysis buffer (50 mM HEPES-KOH pH 7.4, 140 mM
529 NaCl, 1mM EDTA, 1% (v/v) Triton-X-100 and Complete-mini EDTA free protease inhibitor
530 cocktail [Roche]). Cells were lysed with 300 μl acid washed glass beads (425-600 μm) by
531 vigorous agitation for 30 s in a BeadRuptor2 followed by 30 s on ice, repeated 7 times.
532 Sufficient lysis (90%) was confirmed by light microscopy. The lysate was subsequently
533 sonicated at 4°C to obtain an average DNA fragment length of 300 bp. Samples were
534 centrifuged and the supernatant, containing sheared chromatin, recovered.

535 Chromatin was pre-cleared with 20 μl protein A/G magnetic beads (Invitrogen), at 4°C for
536 1 hour. Pre-cleared chromatin was incubated with 10 μg of anti-Sir3 polyclonal IgG
537 antibody (Genscript) or anti-Rap1 polyclonal IgG antibody (Abcam) for 30 min before 25
538 μl of the protein A/G magnetic beads was added. Samples were immuno-precipitated
539 overnight at 4°C with rotation. The supernatant was removed and the beads washed 3×
540 in wash buffer (0.1% [w/v] SDS, 1% [v/v] TritonX-100, 20 mM EDTA, 20 mM Tris-HCl pH

8.0, 150 mM NaCl) followed by 1× wash in wash buffer 2 (0.1% [w/v] SDS, 1% [v/v] TritonX-100, 2 mM EDTA, 20 mM Tris-HCl pH8.0, 500 mM NaCl), and finally resuspended in elution buffer (1% [w/v] SDS, 100 mM $NaHCO_3$). The supernatant was incubated at 65°C with 90 μg proteinase K, 4 h. Samples were subsequently incubated at 37°C, 30 min after the addition of 35 μg RNase A. DNA was purified by phenol-chloroform extraction, precipitated in absolute ethanol, and stored at -80°C.

The Rap1 samples were sequenced using a standard paired-ends protocol described by the manufacturer (Illumina) on a HiSeq250 instrument. For the Sir3 samples, a sequencing library was prepared with a NEXTflex DNA Sequencing kit (PerkinElmer) according to the manufacturer's protocol. End-repaired DNA fragments were ligated to IonCode Barcode Adapters (PerkinElmer), amplified, and sequenced to a median read length of 300 nt on an Ion S5 system. The read quality was assessed and the reads filtered as for the RNA-seq technique, the filtered reads mapped to version 64 of the *S. cerevisiae* reference yeast genome with Bowtie2, and peaks identified relative to a matched input sample with MACS2. The generated bedgraph files were converted to wiggle format, and the total signal in the immune-precipitated and input files adjusted to the identical sum. An identical normalisation was performed for different strains to allow cross comparison. The ChIP-seq analysis was performed on two biological replicates. The Rap1 and Sir3 ChIP-seq data were deposited in the NCBI GEO archive (accession numbers GSE141306 and GSE141317, respectively).

Data analysis and statistics

Various C++ and Python 3 programs and scripts were developed to perform data conversions and analyses, and are all available from http://www.github.com/hpatterton. Get_seqs_from_fastq was used to count the number of occurrences of each histone mutant barcode in a FASTQ file. GO category enrichment was determined with GOrilla[52] and pathway analysis with KEGG Mapper[53]. Bedgraph files generated by MACS2 were converted to wiggle format and normalized with the convert_bedgraph_to_wiggle and normalize_wiggle programs.

Conflict of interest

None to declare

Acknowledgements

This work was partially supported by the National Institutes of Health (Grant 1U01HG007465, to HGP). The funding body did not contribute to the design of the study, collection, analysis, and interpretation of data, or to writing the manuscript. We thank Junbiao Dai for providing reconstructed WT JD47 yeast strain, Dawie van Niekerk for advice on binding equilibria, and Riaan de Witt for critical reading of the manuscript.

Contributions

MN performed the mutant library culturing and bar-code sequencing, chronological lifespan verification, RNA-seq and Rap1 ChIP-seq experiment and edited the manuscript, JR performed the Sir3 ChIP-seq experiment and edited the manuscript. HGP conceived

581 and managed the project, analysed the data, prepared the figures, coded programs where

582 required, and wrote the paper.

583

584 **References**

585 1. Johnson, S. C., Rabinovitch, P. S. & Kaeberlein, M. mTOR is a key modulator of
586 ageing and age-related disease. *Nature* **493**, 338–345 (2013).

587 2. Kourtis, N. & Tavernarakis, N. Cellular stress response pathways and ageing:
588 intricate molecular relationships. *EMBO J.* **30**, 2520–31 (2011).

589 3. Lin, S.-J. *et al.* Calorie restriction extends Saccharomyces cerevisiae lifespan by
590 increasing respiration. *Nature* **418**, 344–348 (2002).

591 4. Longo, V. D. & Fabrizio, P. Chronological Aging in Saccharomyces cerevisiae.
592 *Subcell. Biochem.* **57**, 101–121 (2012).

593 5. Medvedik, O., Lamming, D. W., Kim, K. D. & Sinclair, D. A. MSN2 and MSN4 link
594 calorie restriction and TOR to sirtuin-mediated lifespan extension in
595 Saccharomyces cerevisiae. *PLoS Biol.* **5**, e261 (2007).

596 6. Barros, M. H., Bandy, B., Tahara, E. B. & Kowaltowski, A. J. Higher respiratory
597 activity decreases mitochondrial reactive oxygen release and increases life span in
598 Saccharomyces cerevisiae. *J. Biol. Chem.* **279**, 49883–49888 (2004).

599 7. Pellegrino, M. W., Nargund, A. M. & Haynes, C. M. Signaling the mitochondrial
600 unfolded protein response. *Biochim. Biophys. Acta - Mol. Cell Res.* **1833**, 410–416
601 (2013).

602 8. Tyler, J. K. & Johnson, J. E. The role of autophagy in the regulation of yeast life

span. *Ann. N. Y. Acad. Sci.* **1418**, 31–43 (2018).

9. Pal, S. & Tyler, J. K. Epigenetics and aging. *Sci. Adv.* **2**, e1600584 (2016).

10. Liu, L. *et al.* Chromatin modifications as determinants of muscle stem cell quiescence and chronological aging. *Cell Rep.* **4**, 189–204 (2013).

11. Gross, D. S. & Garrard, W. T. Nuclease Hypersensitive Sites in Chromatin. *Annu. Rev. Biochem.* **57**, 159–197 (1988).

12. Booth, L. N. & Brunet, A. The aging epigenome. *Mol. Cell* **62**, 728–744 (2016).

13. Kaeberlein, M., McVey, M. & Guarente, L. The SIR2/3/4 complex and SIR2 alone promote longevity in Saccharomyces cerevisiae by two different mechanisms. *Genes Dev.* **13**, 2570–2580 (1999).

14. Burnett, C. *et al.* Absence of effects of Sir2 overexpression on lifespan in C. elegans and Drosophila. *Nature* **477**, 482–485 (2011).

15. Tian, X. *et al.* SIRT6 Is Responsible for More Efficient DNA Double-Strand Break Repair in Long-Lived Species. *Cell* **177**, 622-638.e22 (2019).

16. Sen, P. *et al.* H3K36 methylation promotes longevity by enhancing transcriptional fidelity. *Genes Dev.* **29**, 1362–1376 (2015).

17. Dang, W. *et al.* Histone H4 lysine 16 acetylation regulates cellular lifespan. *Nature* **459**, 802–807 (2009).

621 18. Austriaco, N. R. J. & Guarente, L. P. Changes of telomere length cause reciprocal
622 changes in the lifespan of mother cells in Saccharomyces cerevisiae. *Proc. Natl.*
623 *Acad. Sci. U. S. A.* **94**, 9768–9772 (1997).

624 19. Walter, D., Matter, A. & Fahrenkrog, B. Loss of histone H3 methylation at lysine 4
625 triggers apoptosis in Saccharomyces cerevisiae. *PLoS Genet.* **10**, e1004095
626 (2014).

627 20. Oh, S., Suganuma, T., Gogol, M. M. & Workman, J. L. Histone H3 threonine 11
628 phosphorylation by Sch9 and CK2 regulates chronological lifespan by controlling
629 the nutritional stress response. *Elife* **7**, (2018).

630 21. Hayano, M. *et al.* DNA Break-Induced Epigenetic Drift as a Cause of Mammalian
631 Aging. *bioRxiv* 808659 (2019). doi:10.1101/808659

632 22. Yang, J.-H. *et al.* Erosion of the Epigenetic Landscape and Loss of Cellular Identity
633 as a Cause of Aging in Mammals. *bioRxiv* 808642 (2019). doi:10.1101/808642

634 23. Dai, J. *et al.* Probing Nucleosome Function: A Highly Versatile Library of Synthetic
635 Histone H3 and H4 Mutants. *Cell* **134**, 1066–1078 (2008).

636 24. Allen, C. *et al.* Isolation of quiescent and nonquiescent cells from yeast stationary-
637 phase cultures. *J. Cell Biol.* **174**, 89–100 (2006).

638 25. Smith, A. M. *et al.* Quantitative phenotyping via deep barcode sequencing. *Genome*
639 *Res.* **19**, 1836–1842 (2009).

640 26. Burtner, C. R., Murakami, C. J., Kennedy, B. K. & Kaeberlein, M. A molecular
641 mechanism of chronological aging in yeast. *Cell Cycle* **8**, 1256–1270 (2009).

642 27. Fry, C. J., Norris, A., Cosgrove, M., Boeke, J. D. & Peterson, C. L. The LRS and
643 SIN domains: two structurally equivalent but functionally distinct nucleosomal
644 surfaces required for transcriptional silencing. *Mol. Cell. Biol.* **26**, 9045–9059
645 (2006).

646 28. Armache, K.-J., Garlick, J. D., Canzio, D., Narlikar, G. J. & Kingston, R. E. Structural
647 basis of silencing: Sir3 BAH domain in complex with a nucleosome at 3.0 Å
648 resolution. *Science* **334**, 977–982 (2011).

649 29. Wang, F. *et al.* Heterochromatin protein Sir3 induces contacts between the amino
650 terminus of histone H4 and nucleosomal DNA. *Proc Natl Acad Sci U S A* **110**, 8495–
651 8500 (2013).

652 30. Mei, Q. *et al.* Set1-catalyzed H3K4 trimethylation antagonizes the HIR/Asf1/Rtt106
653 repressor complex to promote histone gene expression and chronological life span.
654 *Nucleic Acids Res.* **47**, 3434–3449 (2019).

655 31. Zhu, X. & Gustafsson, C. M. Distinct Differences in Chromatin Structure at
656 Subtelomeric X and Y' Elements in Budding Yeast. *PLoS One* **4**, e6363 (2009).

657 32. Wahlin, J. & Cohn, M. Saccharomyces cerevisiae RAP1 binds to telomeric
658 sequences with spatial flexibility. *Nucleic Acids Res.* **28**, 2292–2301 (2000).

659 33. Platt, J. M. *et al.* Rap1 relocalization contributes to the chromatin-mediated gene
660 expression profile and pace of cell senescence. *Genes Dev.* **27**, 1406–1420 (2013).

661 34. Garay, E. *et al.* High-resolution profiling of stationary-phase survival reveals yeast
662 longevity factors and their genetic interactions. *PLoS Genet.* **10**, e1004168 (2014).

663 35. Powers, R. W. 3rd, Kaeberlein, M., Caldwell, S. D., Kennedy, B. K. & Fields, S.
664 Extension of chronological life span in yeast by decreased TOR pathway signaling.
665 *Genes Dev.* **20**, 174–184 (2006).

666 36. Elgin, S. C. R. & Reuter, G. Position-effect variegation, heterochromatin formation,
667 and gene silencing in Drosophila. *Cold Spring Harb. Perspect. Biol.* **5**, a017780
668 (2013).

669 37. Jona, G., Choder, M. & Gileadi, O. Glucose starvation induces a drastic reduction
670 in the rates of both transcription and degradation of mRNA in yeast. *Biochim.*
671 *Biophys. Acta* **1491**, 37–48 (2000).

672 38. Walsh, M. Characterisation of novel Histone H3 RAD9 mutants defective in the
673 DNA damage response in Saccharomyces cerevisiae. (National University of
674 Ireland, 2013).

675 39. Mei, Q. *et al.* Set1-catalyzed H3K4 trimethylation antagonizes the HIR/Asf1/Rtt106
676 repressor complex to promote histone gene expression and chronological life span.
677 *Nucleic Acids Res.* **47**, 3434–3449 (2019).

678 40. Fabrizio, P., Pozza, F., Pletcher, S. D., Gendron, C. M. & Longo, V. D. Regulation
679 of longevity and stress resistance by Sch9 in yeast. *Science* **292**, 288–290 (2001).

680 41. Hibbs, M. A. *et al.* Exploring the functional landscape of gene expression: directed
681 search of large microarray compendia. *Bioinformatics* **23**, 2692–2699 (2007).

682 42. Huang, H. *et al.* HistoneHits: a database for histone mutations and their
683 phenotypes. *Genome Res.* **19**, 674–681 (2009).

684 43. Smeal, T., Claus, J., Kennedy, B., Cole, F. & Guarente, L. Loss of Transcriptional
685 Silencing Causes Sterility in Old Mother Cells of S. cerevisiae. *Cell* **84**, 633–642
686 (1996).

687 44. Ozaydin, B. & Rine, J. Expanded roles of the origin recognition complex in the
688 architecture and function of silenced chromatin in Saccharomyces cerevisiae. *Mol.*
689 *Cell. Biol.* **30**, 626–639 (2010).

690 45. Kueng, S., Oppikofer, M. & Gasser, S. M. SIR Proteins and the Assembly of Silent
691 Chromatin in Budding Yeast. *Annu. Rev. Genet.* **47**, 275–306 (2013).

692 46. Oppikofer, M. *et al.* Dimerization of Sir3 via its C-terminal winged helix domain is
693 essential for yeast heterochromatin formation. *EMBO J.* **32**, 437–449 (2013).

694 47. Valenzuela, L., Dhillon, N. & Kamakaka, R. T. Transcription independent insulation
695 at TFIIIC-dependent insulators. *Genetics* **183**, 131–148 (2009).

696 48. van Leeuwen, F., Gafken, P. R. & Gottschling, D. E. Dot1p modulates silencing in

yeast by methylation of the nucleosome core. *Cell* **109**, 745–756 (2002).

49. Meneghini, M. D., Wu, M. & Madhani, H. D. Conserved histone variant H2A.Z protects euchromatin from the ectopic spread of silent heterochromatin. *Cell* **112**, 725–736 (2003).

50. Sampath, V. *et al.* Mutational analysis of the Sir3 BAH domain reveals multiple points of interaction with nucleosomes. *Mol. Cell. Biol.* **29**, 2532–45 (2009).

51. Cole, H. A., Howard, B. H. & Clark, D. J. Genome-wide mapping of nucleosomes in yeast using paired-end sequencing. *Methods in enzymology* **513**, 145–68 (2012).

52. Eden, E., Navon, R., Steinfeld, I., Lipson, D. & Yakhini, Z. GOrilla: a tool for discovery and visualization of enriched GO terms in ranked gene lists. *BMC Bioinformatics* **10**, 48 (2009).

53. Kanehisa, M., Goto, S., Sato, Y., Furumichi, M. & Tanabe, M. KEGG for integration and interpretation of large-scale molecular data sets. *Nucleic Acids Res.* **40**, D109-14 (2012).

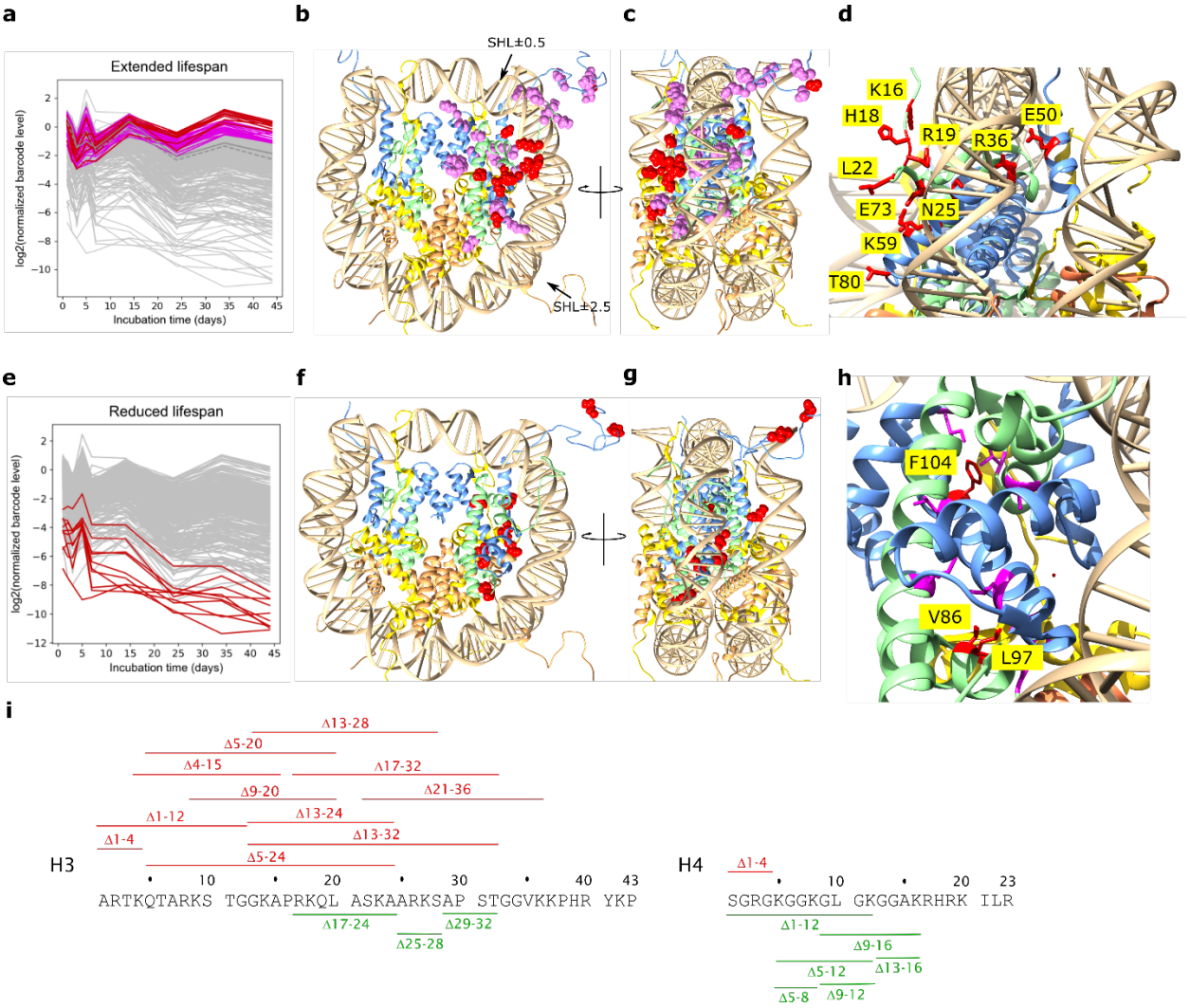

714

715 **Fig 1. Chronological lifespan of histone mutants.** The barcode level of each of the
716 approximately 400 tagged histone mutant strains was determined by sequencing in the
717 quiescent pool at different times in stationary phase, and expressed as $\log_2$ relative to the
718 level at the start of stationary phase (6d), and adjusted to the population median. The $\log_2$
719 ratios of the top 10 individual (red) and top 10% (violet) of strains with most extended
720 lifespan (**a**) and bottom 10 individual strains (red) with most reduced lifespan (**e**) are
721 shown at progressive times of incubation. The trace of the $\log_2$ levels of the parental WT
722 and median strain are shown by solid and dashed dark grey lines respectively (**a**). The

723 residues implicated in the top 10 individual and top 10% of strains that exhibit extended
724 lifespans are shown in red and violet sphere conformation in the structure of the
725 nucleosome (1KX5), respectively (**b**), and the bottom 10 individual strains with the most
726 reduced lifespans are shown in red sphere conformation (**f**). The positions of superhelix
727 locations (SHL) ±0.5 and ±2.5 aligned with the Sin and Lrs sectors[27] are indicated by
728 arrows (**b**). The structures in **b** and **f** are shown rotated by 90° clockwise viewed from
729 the top (**c**,**g**). The 10 individual residues associated with most extended (**d**) and most
730 reduced (**h**) lifespan are shown in stick conformation with individual residues identified.
731 The deletions of sections of the N-terminal tails of H3 and H4 that are associated with
732 extended (green) or reduced (red) CL are indicated (**i**).

733

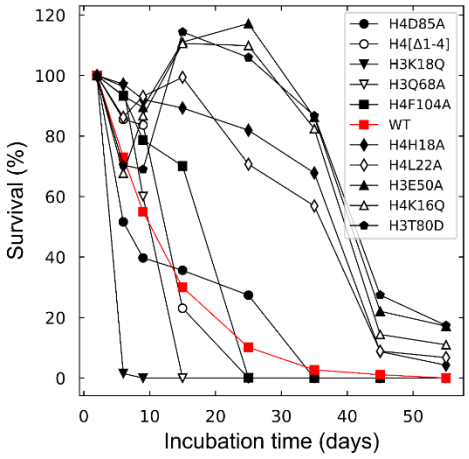

734

735 **Fig. 2. Growth curve of selected strains with extended and truncated lifespans.**
736 Strains with extended or shortened lifespans were selected and cultured individually for
737 up to 55 days. The cell density of each strain was determined at different times, and the
738 percentage cells remaining relative to the starting culture is shown at the different culture
739 times. The strain with the *WT* histones H3 and H4 are indicated by the red plot. Each data
740 point is the average of biological duplicates.

741

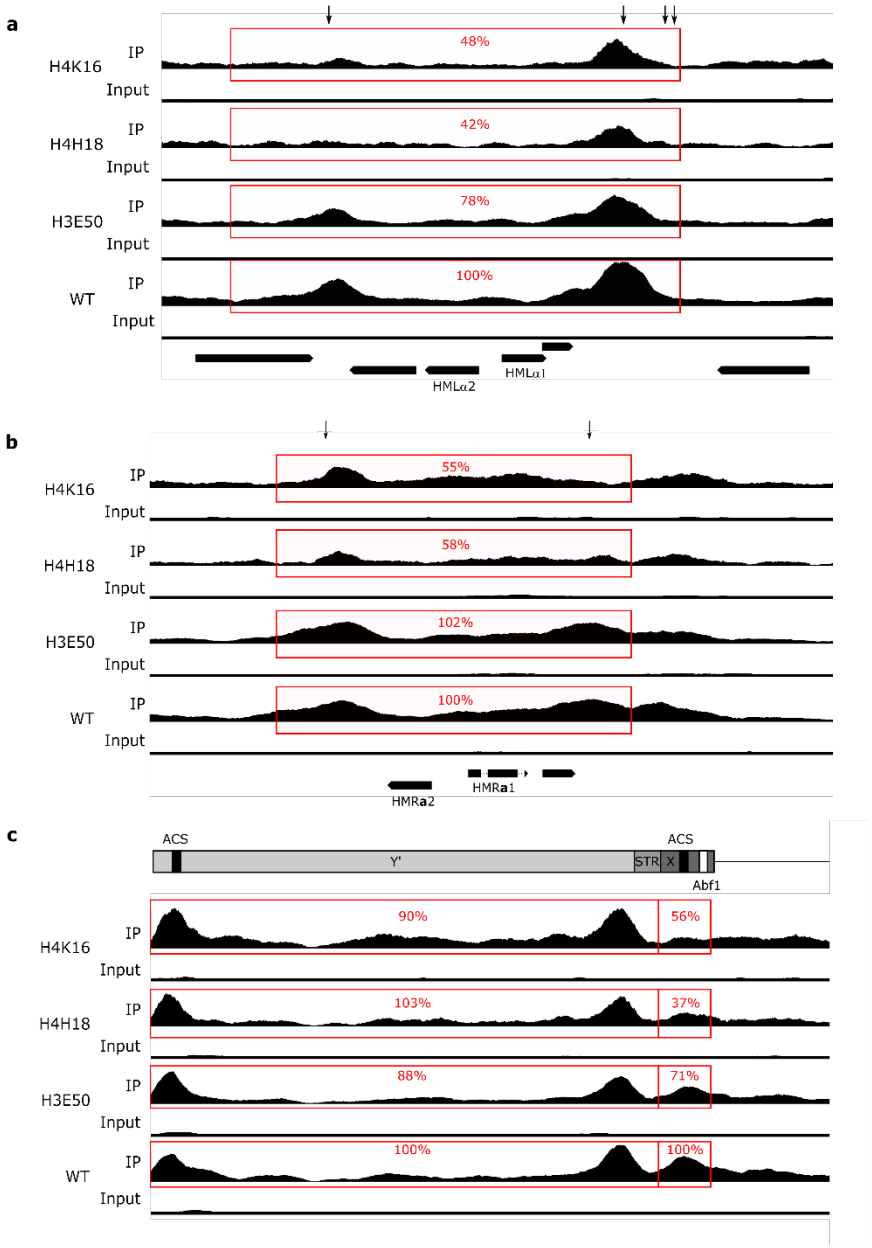

742

743 **Fig. 3. Redistribution of Sir3 in mutant strains.** The genomic distribution of Sir3 was
744 determined for the H4K16Q, H4H18A, H3E50A and WT strains. The immuno-precipitated
745 and input signal, normalised to a ratio of 1, is shown for each strain at the HMLα (**a**),
746 HMRa (**b**) and left telomere of chromosome IX (**c**). The arrows indicate the positions of
747 autonomously replicating consensus sequences (ACSs). The percentage of the pull-

748 down signal relative to the WT strain is shown for each track (representative for biological
749 replicates, n=2). The positions of the MATα1, MATα2, MATa1 and MATa2 genes are
750 indicated. The line diagram at the top of panel **c** shows the location of the X and Y'
751 telomeric elements, the ACSs, Abf1 binding site and sub-telomeric repeat sequences
752 (STR).

753

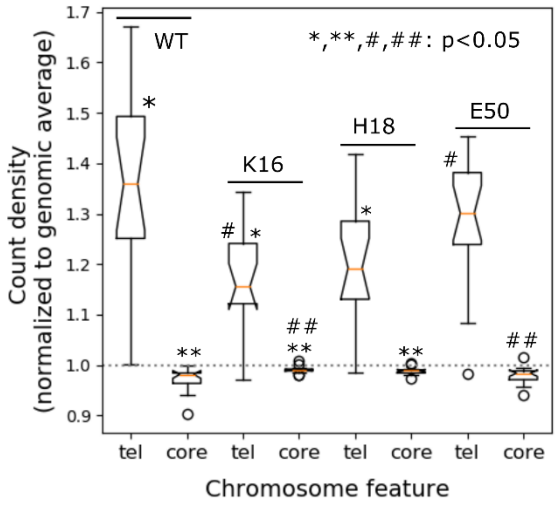

754

755 **Fig. 4. Distribution of Sir3 between telomeres and chromosome cores.** The level of
756 Sir 3 associated with the 20kb chromosome termini and the internal core regions
757 excluding the 20 kb termini were determined from the ChIP-seq signal for each of the 16
758 chromosomes, and normalised to the genome average. The values are shown for the
759 WT and H4K16Q, H4H18A and H3E50A mutant strains. The box plots represent the
760 inter-quartile range (IQR), the notch represents the significance at p<0.05, the orange line
761 shows the median, and the whiskers is shown at 1.5× the IQR. Outliers are shown as
762 individual data points. WT and mutants strains and mutant-mutant strain pairs that are
763 significantly different (*t*-test; p<0.05) in the telomeric and core regions are indicated by
764 the * and # and by ** and ## symbol pairs, respectively.

765

766

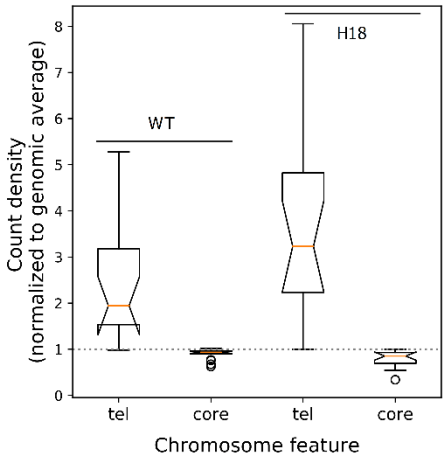

767

768 **Fig. 5. Rap1 binding in the genome.** The level of Rap1 bound to the 20kb chromosome
769 termini (tel) and the internal core regions excluding the termini (core) were determined
770 from the ChIP-seq signal for each of the 16 chromosomes, and normalised to the genome
771 average. The values are shown for the WT and H4H18A mutant strains. The box plots
772 represent the inter-quartile range (IQR), the notch represents the significance at $p<0.05$,
773 the orange line shows the median, and the whiskers is shown at 1.5× the IQR. Outliers
774 are shown as individual data points.

775

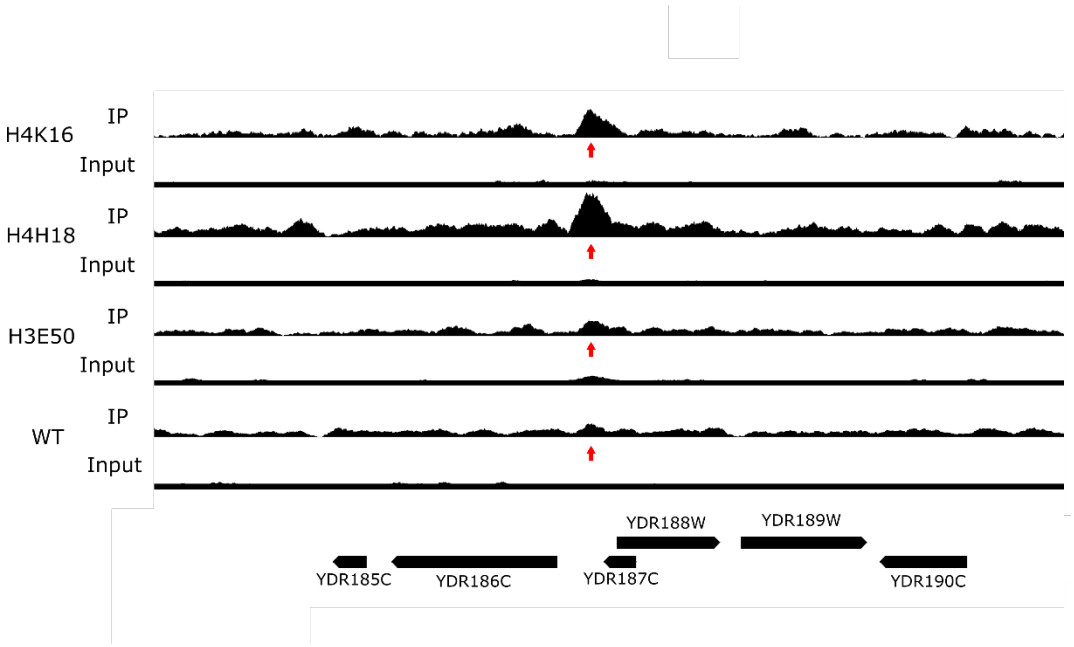

Fig. 6. Binding of Sir3 to secondary loci in the genome. The normalised level of bound Sir3 in a region of the right arm of chromosome IV is shown for the H4K16Q, H4H18A, H3E50A and WT strains. The arrow identifies a Sir3 peak present upstream of the YDR186C (SND1) gene in the H4K16Q and H4H18A strains, but not in the H3E50A or WT strains.

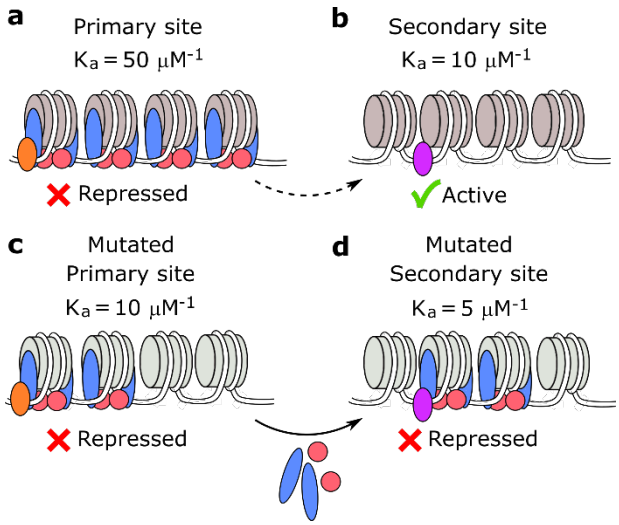

Fig. 7. A model for the redistribution of Sir3 in the genome of some histone mutant strains. The Sir3/Sir4 complex is recruited to a high-affinity binding site by a DNA bound factor to form a heterochromatin domain that represses the covered gene (**a**). The affinity of Sir3/Sir4 for the secondary binding site is significantly less, and little or no Sir3/Sir4 complex binds to this site, allowing the associated gene to remain transcriptionally active (**b**). The mutation of a residue on the nucleosome face that interacts with Sir3 decreases the affinity for the primary binding site significantly (**c**). Although the affinity of the secondary binding sites also decreases, the presence of a different DNA bound factor at this site may modulate this decrease (**d**). The comparable affinities of the mutated primary and secondary binding sites allow Sir3/Sir4 to migrate from primary to secondary binding sites, causing repression of genes associated with the secondary binding sites (**d**).